Journal of Fluorescence, Vol. 10, No. 4, 2000

Steady-State and Time-Resolved Fluorescence Polarization Behavior of Acenaphthene

Trevor A. Smith,[1,2] David J. Haines,[1] and Kenneth P. Ghiggino[1]

Received December 28, 1999; revised April 28, 2000; accepted May 1, 2000

Steady-state and time-resolved fluorescence polarization studies have been carried out on acenaphthene (ACE) in low-temperature glass solutions and at room temperature. In the low-temperature glass the fluorescence polarization values vary considerably with both emission and excitation wavelength. There is a time dependence (on the nanosecond time scale) of the fluorescence anisotropy, $r(t)$, at 77 K, which has a strong dependence upon the excitation and emission wavelengths. Under these conditions, the time-dependent decay of the anisotropy is not attributable to chromophoric motion. The observations are consistent with emission from two closely lying and interconverting excited states. Rate constants for the photophysical processes involved have been determined by fitting the data using a model proposed by Fleming *et. al.* The results are discussed with particular reference to the care required in using dynamic fluorescence polarization measurements to determine energy transfer rates in systems containing this chromophore.

KEY WORDS: Time-resolved fluorescence anisotropy; fluorescence polarization; acenaphthene.

INTRODUCTION

Fluorescence anisotropy measurements are powerful tools in the study of a range of processes that can lead to a loss in the degree of polarization of fluorescence, including molecular motion/rotation and excitation energy transport phenomena. Extending these measurements into the time domain [time-resolved fluorescence anisotropy measurements (TRAMS)] can provide invaluable additional information relating to the dynamics of these processes. For example, the TRAMS technique is often considered to provide the most conclusive evidence for energy migration in molecular arrays such as synthetic vinyl aromatic polymers and allows the kinetics of this process to be determined [1,2]. The applicability of TRAMS to energy migration studies relies on the depolarization of emission arising from multiple chromophore–chromophore energy transfer steps. These studies are usually carried out in solid matrices such as polymer films or low-temperature rigid glasses to observe excitation energy transport in the absence of the emission depolarizing effects of chromophoric rotational motion.

A prerequisite for interpreting the dynamics of energy migration in multichromophoric systems is that the time-resolved fluorescence polarization behavior of a model, single-chromophore compound must first be fully characterized under the same conditions. One such chromophore, acenaphthene (ACE; Fig. 1), is a model compound for polymers derived from the monomer acenaphthylene. These polymers have been studied extensively [2–7] and the results of these works have provided strong evidence for efficient and rapid excitation energy migration.

In this paper we report results obtained from steady-state and time-resolved fluorescence polarization studies of ACE both in a low-temperature glass and at room temperature. Unusual fluorescence polarization behavior

[1] Photophysics Laboratory, School of Chemistry, University of Melbourne, Parkville, Victoria, Australia, 3010.
[2] To whom correspondence should be addressed. e-mail: t.smith@chemistry.unimelb.edu.au

1053-0509/00/1200-0365$18.00/0

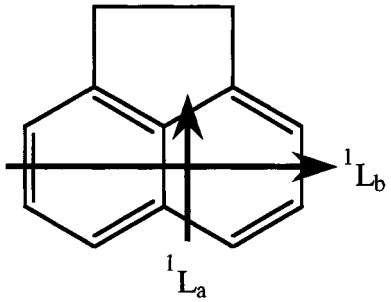

Fig. 1. Structure of acenaphthene (ACE) showing the short (^1L_a) and long (^1L_b) axis-polarized transitions.

was observed which has important implications for the interpretation of fluorescence data from polymers containing this chromophore.

EXPERIMENTAL

Fluorescence decay data were collected by the technique of time-correlated single-photon counting (TCPSC) [8] using as an excitation source the frequency-doubled output of a cavity-dumped rhodamine 6G or DCM dye laser (Spectra Physics 3500) pumped synchronously by a mode-locked argon ion laser (Spectra Physics 2030). The fluorescence was collected by an *f*1 quartz lens (Melles Griot), spectrally selected using a monochromator (Jobin Yvon H10), and detected with a microchannel plate photomultiplier (Hamamatsu R1564U-01). Time-resolved fluorescence anisotropy measurements were carried out by collecting decays with the emission polarization analyzer set parallel and then perpendicular to the direction of the (vertical) polarization of the excitation light. The emission polarization analyzer was switched between the parallel and the perpendicular positions for preset periods (usually 30-s dwell times) and the two decays were collected in separate 512 channel memories of a multichannel analyzer (Tracor Northern ECON II) over total collection periods exceeding an hour to enhance the signal-to-noise ratio of the anisotropy function.

The time-resolved fluorescence anisotropy function, $r(t)$, is calculated using Eq. (1), in which $I_{\parallel}(t)$ and $I_{\perp}(t)$ are the individual decays collected with the polarization analyzer set parallel and perpendicular to the vertically polarized excitation light. The "*G*" factor is included to account for any polarization bias of the detection system. The influence of this term was minimized by arranging the polarization analyzer to be the first element in the detection system and using a polarization scrambler immediately prior to the emission monochromator.

$$r(t) = \frac{I_{\parallel}(t) - GI_{\perp}(t)}{I_{\parallel}(t) + 2GI_{\perp}(t)} \quad (1)$$

2-Methyl tetrahydrofuran (MTHF; Aldrich; 99%) was thoroughly dried and purified by repeated refluxing and distillation until no impurity fluorescence was detectable at the relevant excitation wavelengths. This solvent forms a clear glass at $\sim$ 90 K and is transparent at the excitation wavelengths required to excite ACE [9,10]. ACE (Hopkins & Williams, G.P.R.) was purified by repeated recrystallizations from spectroscopic-grade ethanol [11]. The optical density of ACE in MTHF was kept to 0.05 at 295 nm (corresponding to a concentration of $\sim 10^{-5}$ *M*) to minimize interchromophore effects. Low-temperature measurements were carried out in a liquid nitrogen cryostat (OptiStat DN; Oxford Instruments) with an ITC601 controller. Samples were contained in specially constructed quartz fluorescence cuvettes and were degassed thoroughly using multiple freeze–pump–thaw cycles (to 10^{-7} Torr). Steady-state fluorescence polarization spectra were recorded using an Hitachi 4500 spectrofluorimeter equipped with a fluorescence polarization accessory and using excitation and emission bandpass values of 3 nm. Polarization excitation–emission matrices were recorded by sequentially scanning the emission monochromator as a function of excitation wavelength and polarization analyzer position.

Data analyses, fitting the functions discussed below, were carried out on a Pentium PC running MicroSoft Excel and employing the built-in Solver function [12]. The routine used allows the various parameters of user-defined functions to be adjusted while iteratively minimizing a function representing the reduced chi-square calculated from the sum of the squares of the differences between the calculated curve and the experimental data. The Solver function also allows for the constraint of any parameters to within user-defined limits. Convolution of the instrument response function with the fitted curve was not considered to be necessary, taking into account the time scales of the measurements and the narrow width of the instrument response function ($\sim$100-ps FWHM), and so was not incorporated in this analysis.

RESULTS AND DISCUSSION

Steady-State Measurements

Acenaphthene can be considered as a 1,8-disubstituted naphthalene and its absorption spectrum is similar to that of 1,8,-dimethylnaphthalene [13]. Accordingly, the absorption centered around 295 nm is associated with the

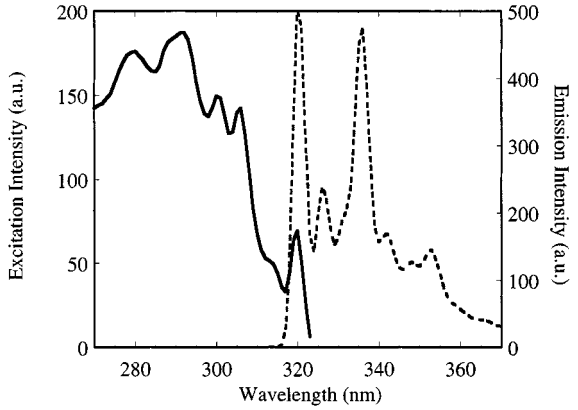

Fig. 2. Fluorescence excitation and emission spectra λ_{ex} = 295 nm) of ACE at 77 K.

short-axis (transverse) polarized ^1L_a S_0–S_2 transition and the weaker absorption near ~330 nm is due to the forbidden, long-axis (longitudinally) polarized ^1L_b S_0–S_1 transition (Fig. 1). The absorption and emission spectra of ACE in MTHF at liquid nitrogen temperature are shown in Fig. 2 and exhibit a pronounced vibronic structure.

Values for many of the photophysical parameters for ACE have been collated by Murov [9]. The fluorescence quantum yield, ϕ_f, of ACE is reasonably insensitive to temperature, being 0.50 in cyclohexane [14] (cf. ~0.39 in ethanol [15] at room temperature and 0.57 in an EPA (5:5:2 diethylether:isopentane:ethanol) glass at 77 K) [16]. The fluorescence lifetime, τ_f, of ACE at room temperature in cyclohexane is reported to be 46 ns [17].

The steady-state polarized fluorescence excitation and emission spectra of ACE in MTHF glass at 77 K are shown in Fig. 3. In the low-temperature glass, the

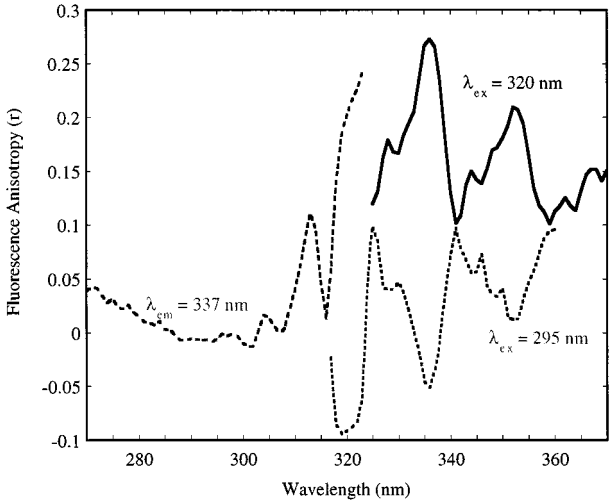

Fig. 3. Polarized emission (λ_{ex} = 295 and 320 nm) and excitation spectra (λ_{em} = 337 nm) of ACE in MTHF at 77 K.

fluorescence anisotropy shows a strong dependence on both the excitation and the emission wavelengths including negative values at certain wavelengths. Complex fluorescence behavior is often best analyzed through excitation–emission matrices (EEMs) generated by the use of total (or synchronous) luminescence spectroscopy. Steady-state *fluorescence anisotropy* EEMs, in which a "three-dimensional" overview of the fluorescence polarization behavior is displayed as topometric (hypersurface) and/or contour diagrams, have been reported [18], however, the full potential of these measurements appears to be largely untapped in the literature. Such polarization excitation/emission contour diagrams seem ideally suited for illustrating the complex fluorescence polarization behavior exhibited by molecules such as ACE, and an example of this is shown in Fig. 4. The expected anisotropy value for a given combination of these wavelengths is apparent and the most appropriate excitation and emission wavelengths for subsequent fluorescence polarization experiments can be selected at a glance. The maximum anisotropy value recorded over the entire excitation/emission matrix is seen to be ~0.1 (excluding the region of scattered light in the bottom left-hand corner in Fig. 4), whereas a minimum of less than −0.08 is observed at $\lambda_{ex} \approx 290$ nm and $\lambda_{em} \approx 322$ nm. It is evident that the negative anisotropy is associated with the two main vibronic emission bands at ~322 and 337 nm (Fig. 2) within the excitation range ~280 to 308 nm. Other weaker emission bands at ~326, ~330, ~342, ~347, and ~352 nm exhibit positive anisotropy values across the excitation range, and the magnitude of the anisotropy is unrelated to the emission intensity, with the bands at 326 and 342 nm displaying the highest anisotropy values. Figure 4 therefore provides a clear overview of the fluorescence anisotropy behavior exhibited by this system and illustrates the potential of plots of this sort to provide a wealth of information in a compact form.

Fluorescence anisotropy is usually observed to be independent of the emission wavelength, since fluorescence usually originates from the lowest singlet state following rapid internal conversion from upper excited levels, so only polarized *excitation* spectra are usually reported [19]. In the present example, however, the pronounced structure in the polarized *emission* spectra suggests that the radiative transitions involve contributions from more than one state with different intrinsic polarization behavior. The polarized fluorescence excitation spectra reported here can be compared with the results of David *et al.* [20], who, by comparison with naphthalene [21,22], attributed the wavelength-dependent behavior of the excitation spectra of ACE to two series of vibrational levels polarized in opposite directions, with the vibrations

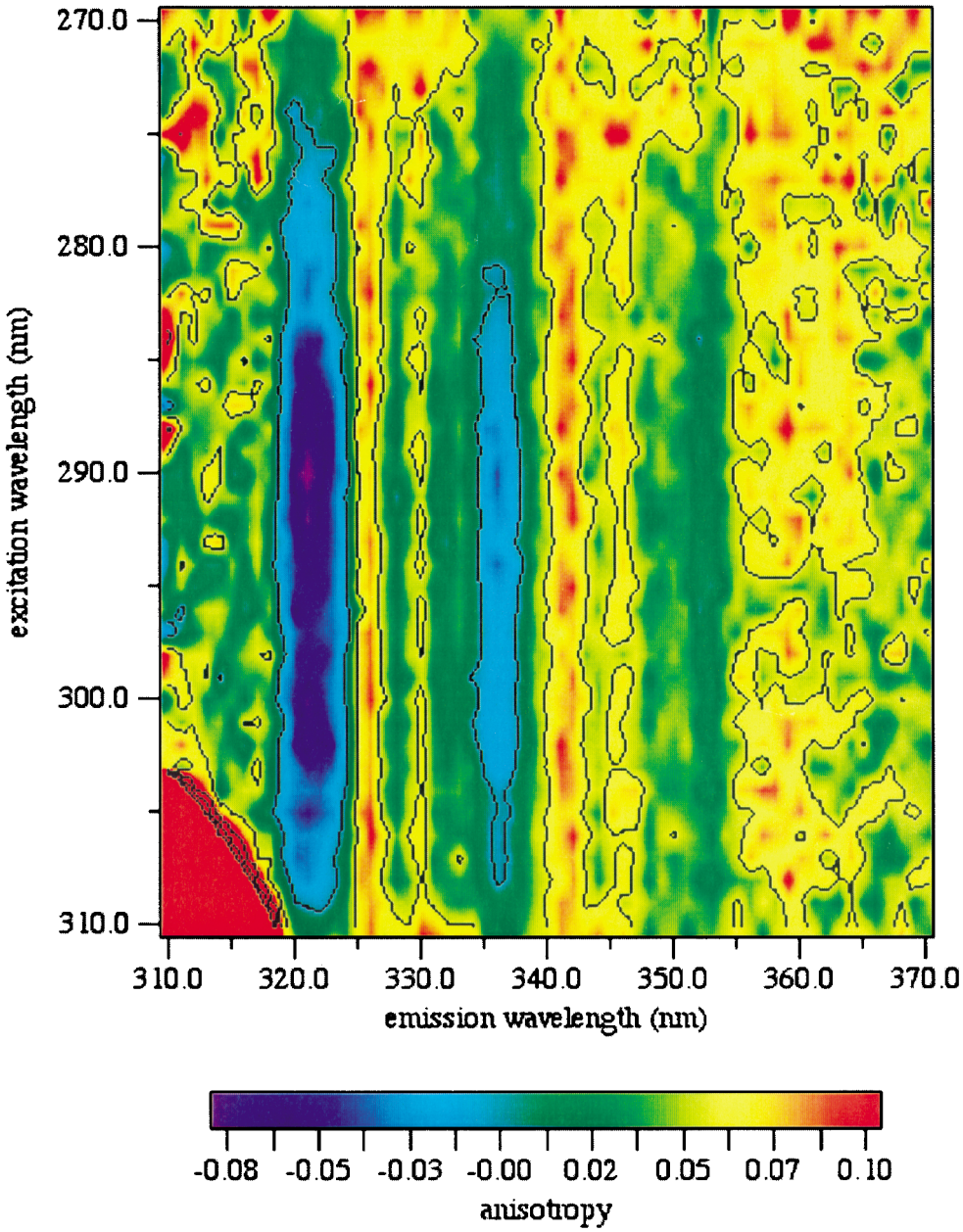

Fig. 4. Fluorescence anisotropy excitation/emission contour plot for ACE in MTHF at 77 K.

at 323 and 337 nm belonging to one series and the vibrations at 327 and 342 nm to the other. The information contained in Fig. 4 lends support to that interpretation.

Time-Resolved Measurements

Fluorescence decays were recorded with the emission polarizer set at the magic angle (54.7°) [23–25] from acenaphthene in MTHF at room temperature and at 77 K using excitation wavelengths of 295 and 320 nm (Table I). One decay time of ~42 ns, in reasonable agreement with that reported elsewhere in cyclohexane [17], is consistent at both temperatures and at both excitation wavelengths. At room temperature, the decays are essentially independent of excitation wavelength and decay exponentially with this characteristic lifetime. In the low-temperature glass, however, the fluorescence decay behavior is more complex. Exciting at 295 nm results in a small

Table I. Magic-Angle Fluorescence Decay Behavior of Acenaphthene in MTHF at Room Temperature and at 77 K[a]

Excitation wavelength (nm)	Temperature (K)	
	293	77
295	τ = 41.2 ns	τ_1 = 7.6 ns, A_1 = 0.06, τ_2 = 41.1 ns, A_2 = 0.94
320	τ = 42.5 ns	τ = 42.6 ns

[a] The emission wavelength in all cases was 337 nm.

contribution from a second exponential term with a lifetime of ~7 ns in addition to the 42-ns decay time, whereas excitation at longer wavelengths (320 nm) again results in a single exponential decay with the characteristic ~42-ns lifetime. The insensitivity of the fluorescence decay time to temperature reflects the quantum yield data mentioned earlier and is probably related to the rigidity of the ACE structure.

The time-resolved fluorescence anisotropy of ACE at room temperature (not shown) exhibits a rapid depolarization of fluorescence within the time resolution of the apparatus associated with the short rotational correlation time of ACE in solution. Of more interest in the current context is the TRAMS behavior in the low-temperature glass, where any contribution to the fluorescence depolarization due to chromophore rotation is removed. Excitation of ACE at 295 nm results in an unexpected but marked decay of $r(t)$ with time, while excitation at the red edge (323 nm) leads to only a very slight anisotropy decay (Fig. 5). There is also a marked excitation and emission wavelength dependence of the limiting anisotropy value [$r(\infty)$], with these values corresponding closely to the values obtained from the steady-state measurements at the corresponding excitation and emission wavelengths. The highest values for the limiting anisotropy were obtained upon excitation into the red edge of the absorption spectrum. That the limiting anisotropy values, $r(\infty)$, obtained on different (steady-state and time-resolved) instruments concur is strong evidence that this effect is not due to any instrumental artifact.

This unexpected time dependence of the fluorescence anisotropy function in this rigid, low-temperature matrix potentially complicates the analysis of similar measurements from acenaphthylene-containing polymers, and so the source of this depolarizing effect requires identification. Energy migration between chromophores is unlikely to be the cause of this effect considering the low concentration of ACE used and the R_o (15.9 Å) [26] for ACE–ACE energy transfer. Furthermore, a randomization of the emission polarization due to interchromophore energy migration would be expected to depolarize the emission completely (as observed in some polymer systems such as poly(acenaphthylene) [27]) rather than leaving a wavelength-dependent, finite (and sometimes negative), limiting anisotropy as observed.

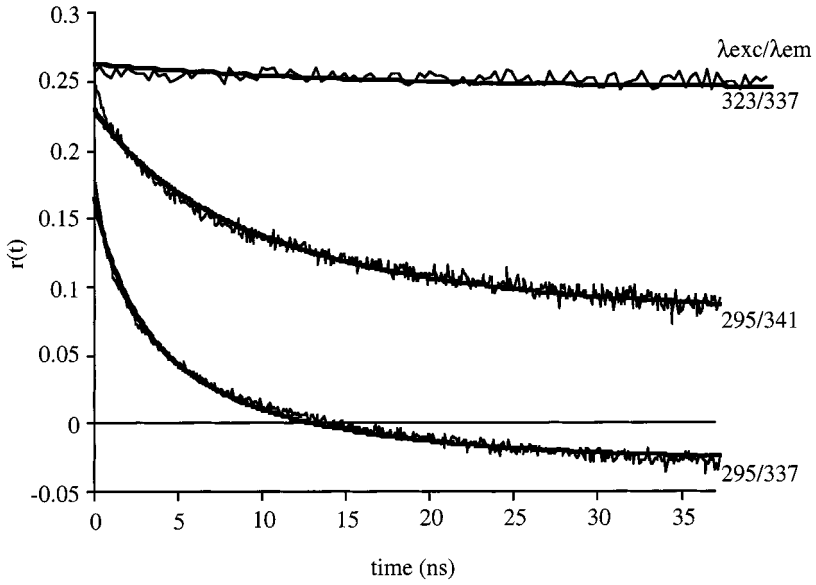

Fig. 5. Time-resolved fluorescence anisotropy profiles of ACE in MTHF at 77 K at various excitation and emission wavelengths as indicated. The lines of best fit are as discussed in the text. Calibration factors are 0.3 ns/ch for the 323/337 curve and 0.081 ns/ch for the two curves with excitation at 295 nm.

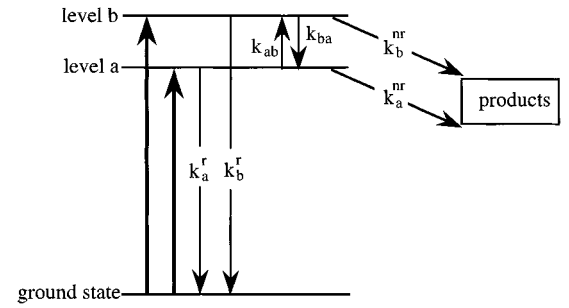

Fig. 6. Schematic energy level diagram for two low-lying excited states.

One interpretation of the observed time-resolved fluorescence decay and fluorescence anisotropy behavior is to consider the emission to be associated with two interconverting excited states. Such a situation has been reported by Fleming *et al.* [28–31] in their investigation of the effects of "level kinetics" on the time-dependent fluorescence polarization behavior of tryptophan in solution on picosecond time scales. The results discussed above suggest that the model developed by Fleming *et al.* derived from the scheme shown in Fig. 6 may also be appropriate for acenaphthene.

Tryptophan has two low-lying ^1L_a and ^1L_b excited states [32] which have transition dipole moments coupling to the ground state which are at large angles to each other and whose absorption spectra overlap in the region between 250 and 300 nm. Fleming *et al.* [28–31] extended the work reported by Andrews and Forster [33] to develop expressions for the time-dependent populations of the two states and the resulting time-resolved fluorescence anisotropy assuming that certain proportions of the two states were initially excited, conversion between the two states could occur, and the monitored emission could arise from either or both states. The analysis of time-resolved polarization spectroscopy reported by Fleming *et al.* was later generalized further by Szabo [34], producing essentially identical results.

The ^1L_a and ^1L_b states of polyacenes are distinguished from each other by the difference in the node distributions of their wave functions [32]. In aromatic hydrocarbons such as 7-azaindole [35], a series of carbazole derivatives [36], anthracene [37], and naphthalene [13,37], semiempirical calculations suggest that the ^1L_a state lies between 2200 and 4100 cm^{-1} above the ^1L_b state in each case, and it is reasonable to assume that this is also the case for acenaphthene. Preliminary CNDO/S calculations on ACE predict that these states are separated by <3100 cm^{-1}, however, in the solution phase and in the low-temperature glass, these two excited states are very likely closer in energy. These preliminary calculations also predict that the dipole moments of the two lowest excited singlet states are 1.83 and 1.41 D, compared with 1.32 D in the ground state.

Following the terminology of Fleming *et al.* [31,38], assuming that the fluorescence decay time and fluorescence quantum yield of the chromophore are known, the following parameters can be defined in terms of the radiative, k_a^r, k_b^r, and nonradiative, k_a^{nr}, k_b^{nr}, rate constants, of levels a and b, respectively.

$$k_a \equiv k_a^r + k_a^{nr} \tag{2}$$

$$k_b \equiv k_b^r + k_b^{nr} \tag{3}$$

$$\delta \equiv k_a + k_{ab} - k_b - k_{ba} \tag{4}$$

$$Q \equiv [\delta^2 + 4k_{ab}\, k_{ba}]^{1/2} \tag{5}$$

$$k \equiv k_a + k_{ab} + k_b + k_{ba} \tag{6}$$

$$\lambda_1 \equiv \frac{-(k - Q)}{2} \tag{7}$$

$$\lambda_2 \equiv \frac{-(k + Q)}{2} \tag{8}$$

The excited-state populations of the two states as a function of time are then given by

$$K^a(t) = \frac{1}{2Q}\{K^a(0)\,[Q - \delta] + 2k_{ba}K^b(0)\}\exp(\lambda_1 t) + \frac{1}{2Q}\{K^a(0)\,[Q + \delta] - 2k_{ba}K^b(0)\}\exp(\lambda_2 t) \tag{9}$$

$$K^b(t) = \frac{1}{2Q}\{K^b(0)\,[Q + \delta] + 2k_{ab}K^a(0)\}\exp(\lambda_1 t) + \frac{1}{2Q}\{K^b(0)\,[Q - \delta] - 2k_{ab}K^a(0)\}\exp(\lambda_2 t) \tag{10}$$

where $K^a(0)$ and $K^b(0)$ are the initial populations of states a and b, i.e., these parameters are proportional to the amount of each state excited initially by the incident laser pulse.

In their original work Fleming *et al.* [28,29] assumed that the absorption and emission transition dipoles that couple the ground state to each excited state were parallel and the transition moments of the two excited states were perpendicular or at large angles to each other. In a later paper Fleming *et al.* [31] extended their model to remove this constraint and thus allow the fluorescence anisotropy resulting from each level and conversion between levels to be calculated as a function of time. According to this model, the time-dependent anisotropy due to each level is given by

$$r^{a}(t)K^{a}(t) = \left(\frac{2}{5}\right)\left(\frac{1}{2Q}\right)[\{K^{a}(0)P_2(\cos\vartheta_{EA}^{aa})[Q-\delta] + 2k_{ba}K^{b}(0)\,P_2(\cos\vartheta_{EA}^{ab})\}\exp[(\lambda_1 - 6D)t]] + \{K^{a}(0)P_2(\cos\vartheta_{EA}^{aa})[Q+\delta] - 2k_{ba}K^{b}(0)\,P_2(\cos\vartheta_{EA}^{ab})\}\exp[(\lambda_2 - 6D)t] \quad (11)$$

$$r^{b}(t)K^{b}(t) = \left(\frac{2}{5}\right)\left(\frac{1}{2Q}\right)[\{K^{b}(0)P_2(\cos\vartheta_{EA}^{bb})[Q+\delta] + 2k_{ab}K^{a}(0)\,P_2(\cos\vartheta_{EA}^{ba})\}\exp[(\lambda_1 - 6D)t]] + \{K^{b}(0)P_2(\cos\vartheta_{EA}^{bb})[Q-\delta] - 2k_{ab}K^{a}(0)\,P_2(\cos\vartheta_{EA}^{ba})\}\exp[(\lambda_2 - 6D)t] \quad (12)$$

(where the $P_2\cos(\vartheta) = \frac{1}{4}(1 + 3\cos 2\vartheta)$ terms correspond to the second Legendre polynomial[39] and take into account the angles between the various absorption and emission transition dipoles of the two levels, *viz.*, ϑ_{EA}^{aa}, ϑ_{EA}^{ab}, ϑ_{EA}^{bb} and ϑ_{EA}^{ba}.

Finally, the total fluorescence anisotropy is given by

$$r(t) = \frac{[k_a^r\, g_a(\omega) r^{a}(t)\, K^{a}(t) + k_b^r\, g_b(\omega) r^{b}(t)\, K^{b}(t)]}{K^{a}(t)k_a^r g_a(\omega) + K^{b}(t)k_b^r g_b(\omega)} \quad (13)$$

where $g_a(\omega)$ and $g_b(\omega)$ are the spectral lineshape functions which define the proportion of the monitored emission emanating from levels a and b, respectively, following excitation of various proportions of the two levels as given by $K^{a}(0)$ and $K^{b}(0)$.

In the present case (as in the work of Fleming *et al.*), it was assumed that the two levels have the same radiative and nonradiative rate constants, i.e., $k_a^r = k_b^r$ and $k_a^{nr} = k_b^{nr}$ [40]. Assuming a fluorescence lifetime of 42 ns (obtained from the magic angle analysis from red-edge excitation discussed above) and fluorescence quantum yield of 0.5[14], all four of these rate constants were thus set to equal $1.19 \times 10^7\ s^{-1}$. The diffusion coefficient, D, incorporated into the original model by Fleming *et al.*, was assumed to be zero for the case of the rigid glass environment. The rate constant for conversion from the lower to the upper level, k_{ab}, could be varied or fixed to zero. The other unknown parameters k_{ba}, the Legendre polynomial terms in ϑ_{EA}^{aa}, ϑ_{EA}^{ab}, ϑ_{EA}^{bb} and, ϑ_{EA}^{ba}, and $g_a(\omega)$, $g_b(\omega)$, $K^{a}(0)$, and $K^{b}(0)$ (for each excitation/emission wavelength) were all varied by nonlinear iterative [12] fitting of Eq. (13) to the experimentally determined anisotropy data while minimizing an effective χ^2 parameter in a "global analysis" approach [41]. That is, k_{ba} and the Legendre polynomial terms were varied but linked across the three $r(t)$ profiles, while individual values for $g_a(\omega)$, $g_b(\omega)$, $K^{a}(0)$, and $K^{b}(0)$ were optimized for each curve. The values of the Legendre polynomial terms were constrained to lie between -0.5 and 1 and the $K^{a}(0)$, $K^{b}(0)$ and $g_a(\omega)$, $g_b(\omega)$ terms were constrained to be ≥ 0.

Figure 5 includes the resulting global best fits of Eq. (13) for the cases of excitation at 295 nm, with emission monitored at 337 and 341 nm, and for excitation at 323 nm, with emission monitored at 337 nm. The 323/337-nm data were recorded over ~150 ns, whereas the other two curves were collected on a time scale of ~40 ns. Only the first ~35 ns of the 323/337-nm curve is shown in Fig. 5, but analysis was over the entire 150 ns of the profile to monitor sufficient decay of the $r(t)_{323/337}$ profile. It is interesting to note that this model can also fit the entire $r(t)$ profile, i.e., it can successfully predict the initial anisotropy value r_0 as being significantly less than the theoretical maximum of 0.4. This was discussed in the paper by Ruggiero *et al.* [31] for tryptophan. Clearly, the data can be described quite well by the model under discussion here, however, this is the case only if the rate constant for conversion from the higher to the lower level is of the order of $10^8\ s^{-1}$ and the rate constant for the opposite transition is at least an order of magnitude lower than this (or fixed to zero). These findings are quite similar to those reported by Ganguly *et al.* [36] for some 2,7-dimethoxycarbazoles, calculated from time-resolved fluorescence measurements recorded at the magic angle. They suggest that the small energy gap and a low density of states isoenergetic with the (higher-energy) ^1L_a state should contribute to causing a slow rate for the $^1L_a \rightarrow {}^1L_b$ radiationless process ($\sim 10^8\ s^{-1}$). A similarly small energy gap between the first and the second levels and a very low density of states in the related molecule, naphthalene, have been discussed [42], and we postulate that this may also be the case in ACE, resulting in the slow rate of conversion from the upper to the lower level.

The recovered angles between the absorption and the emission transition dipoles ϑ_{EA}^{aa}, ϑ_{EA}^{ab}, ϑ_{EA}^{bb}, and ϑ_{EA}^{ba} were ~28, 65, 60, and 40°, respectively. The ratio of the recovered values for the $K^{a}(0)$ and $K^{b}(0)$ terms varies from 19 with excitation at 323 nm to 0.25 with excitation at 295 nm. These values and the data summarized in Table II correspond well with the trends expected from the proposed model. Exciting into the red edge of the absorption (323 nm) populates almost purely the lower-energy state (*a*), and since interconversion from state *a* to state *b* is slow (if occurring at all), almost all the detected emission emanates from the lower level *a*. Excitation at the higher energy (295 nm) populates significantly more of the higher level but the emission is still predominantly from the lower level, with the proportion depending on the emission wavelength monitored. There is still, however, a significant amount of emission arising from the upper level, thus implicating the existence of

Table II. Parameters Used in and Recovered from the Global Analysis of the Three $r(t)$ Profiles Using Eq. (13) Corresponding to the Fits as Shown in Fig. 5[a]

Fixed parameters		Recovered adjustable parameters	
$\phi_{fa} = \phi_{fb}$	0.5	k_{ba}	$7.1 \times 10^7\ s^{-1}$
$k_a = k_b = 1/42$ ns	$2.38 \times 10^7 s^{-1}$	$g_a(\omega)_{295/337}$	88.9%
$k_a^r = k_b^r$	$1.19 \times 10^7\ s^{-1}$	$g_a(\omega)_{295/341}$	76.3%
$k_a^{nr} = k_b^{nr}$	$1.19 \times 10^7\ s^{-1}$	$g_a(\omega)_{323/337}$	99.7%

[a] k_{ab} was fixed to zero; other parameters are as given in the text.

dual emission from ACE in the low-temperature MTHF glass.

This evidence for dual emission is supported by the magic-angle fluorescence decays (Table I). The inclusion of the rate constant k_{ba} in addition to the rate constants k_a^r and k_a^{nr} will, of course, shorten the lifetime of the upper state with respect to the lower-state lifetime. Using the interstate conversion rate constant obtained from the analysis, $k_{ba} = 7 \times 10^7\ s^{-1}$, and the radiative and nonradiative rate constants given above, gives a fluorescence lifetime of the upper level of ~10 ns which is in good agreement with that of the second exponential term obtained from the magic-angle decays upon excitation at 295 nm (Table I).

We note here, in conclusion, that we have also observed similar steady-state and time-resolved fluorescence anisotropy behavior from another aromatic molecule, namely, (9-phenanthryl)methyl pivalate, under the same conditions as reported for ACE. This molecule was synthesized as a model compound for energy migration studies in poly((9-phenanthryl)methyl methacrylate), a polymer in which energy migration might be expected to be efficient due to the much reduced excimer formation reportedly exhibited by phenanthryl groups compared with naphthalene derivatives. The fluorescence anisotropy from this compound was found to decay on a time scale similar to that reported here for ACE. Analysis of the anisotropy decays as a function of emission wavelength, based on the same two-level system under discussion here, provided fits of comparable quality to those reported in this paper for ACE and returned a value for k_{ba} of $\sim 7 \times 10^7\ s^{-1}$, which is again very similar to that discussed above for ACE and the 2,7-dimethoxycarbazoles reported by Ganguly *et al.* [36]. A rigorous analysis for 9PhMP, such as that given above for ACE, is more problematic, however, due to the more complex (triple-exponential) fluorescence decay behavior observed from 9PhMP in MTHF at 77 K compared to ACE under the same conditions.

CONCLUSIONS

The fluorescence anisotropy for the compound acenaphthene has been measured in a low-temperature glass. This molecule exhibits complex fluorescence anisotropy behavior both in the steady state and in the time domain. Extending the use of excitation/emission matrices to illustrate the polarization data is a convenient way of visualizing the steady-state behavior and selecting optimal excitation and emission wavelengths for time-resolved studies. Time-resolved fluorescence anisotropy measurements show an unexpected and marked time dependence. This behavior has been successfully modeled on the basis of emission from, and interconversion between, two close-lying excited states. This behavior has been reported elsewhere for derivatives of anthracene and referred to as an "anti-Kasha" emission [43], in recognition of the apparent violation of Kasha's rule [44] that this interpretation infers. The rate for conversion from the upper to the lower state is found to be surprisingly slow but is in qualitative agreement with that reported for some 2,7-dimethoxycarbazoles. We also report that similar behavior is observed from 9PhMP and postulate that this behavior may be more common than generally assumed. A particular consequence of our studies is that it clearly illustrates that caution is required in the interpretation of fluorescence anisotropy decays from ACE in polymers as arising solely from energy migration. The excitation and emission wavelengths need to be chosen with some care to ensure that any fluorescence anisotropy decay observed truly arises from energy transfer processes.

ACKNOWLEDGMENTS

This work was supported by funds from the Australian Research Council. Technical assistance provided by Nuno Cabral is also gratefully acknowledged.

REFERENCES

1. A. D. Stein, K. A. Peterson, and M. D. Fayer (1990) *J. Chem. Phys.* **92**, 5622–5635.
2. K. P. Ghiggino and T. A. Smith (1993) *Prog. React. Kin.* **18**, 375–436.
3. C. David, M. Lempereur, and G. Geuskens (1972) *Eur. Polym. J.* **8**, 417–427.
4. R. A. Anderson, R. F. Reid, and I. Soutar (1980) *Eur. Polym. J.* **16**, 945–950.
5. C. David, M. Piens, and G. Geuskens (1980) *Eur. Polym. J.* **8**, 1019–1031.

6. W. R. Carbaness, S. A. Zamzam, and C. T. Chen (1987) in C. E. Hoyle and J. M. Torkelson (Eds.) *Photophysics of Polymers*, ACS, Washington, DC, Vol. 358, pp. 358–366.
7. K. P. Ghiggino, E. K. L. Yeow, D. J. Haines, G. D. Scholes, and T. A. Smith (1996) *J. Photochem. Photobiol. A Chem.* **102**, 81–86.
8. D. V. O'Connor and D. Phillips (1983) *Time-Correlated Single Photon Counting*, Academic Press, London.
9. S. L. Murov, I. Carmichael, and G. L. Hug (Eds.) (1993) *Handbook of Photochemistry*, 2nd ed., M. Dekker, New York.
10. B. Brocklehurst and R. N. Young (1994) *J. Chem. Soc. Faraday Trans.* **90**, 271–278.
11. D. D. Perrin and W. L. Armarego (1988) *Purification of Laboratory Chemicals*, 3rd ed., Permagon Press, Sydney.
12. Microsoft Corporation (1997).
13. H. H. Jaffé and M. Orchin (1962) *Theory and Applications of Ultraviolet Spectroscopy*, Wiley & Sons, New York.
14. J. B. Birks (1970) *Photophysics of Aromatic Molecules*, Wiley–Interscience, London.
15. C. A. Parker and T. A. Joyce (1966) *J. Chem. Soc. Faraday Trans.* **62**, 2785–2892.
16. G. Heinrich and H. Güsten (1979) *Z. Phys. Chem. NF* **118S**, 31–41.
17. I. B. Berlman (1971) *Handbook of Fluorescence Spectra of Aromatic Molecules*; 2nd ed., Academic Press, London.
18. K. A. Destrampe and G. A. Hieftje (1990) *Appl. Spectrosc.* **47**, 1548–1554.
19. J. R. Lakowicz (1983) *Principles of Fluorescence Spectroscopy*, Plenum Press, New York.
20. C. David, D. Baeyens-Volant, and M. Piens (1980) *Eur. Polym. J.* **16**, 413–423.
21. H. Zimmermann and N. Joop (1961) *Z. Elektrochem.* **65**, 61–66.
22. H. Zimmermann and N. Joop (1960) *Z. Elektrochem.* **64**, 1215–1219.
23. M. Shintzky (1972) *J. Chem. Phys.* **56**, 5979–5981.
24. G. R. Fleming, J. M. Morris, and G. W. Robinson (1976) *Chem. Phys.* **17**, 91–100.
25. M. G. Badea and L. Brand (1979) *Methods Enzymol.* **61**, 378–425.
26. I. B. Berlman (1973) *Energy Transfer Parameters of Aromatic Compounds*, Academic Press, London.
27. T. A. Smith and K. P. Ghiggino, unpublished results.
28. A. J. Cross, D. H. Waldeck, and G. R. Fleming (1983) *J. Chem. Phys.* **78**, 6455–6467.
29. A. J. Cross, D. H. Waldeck, and G. R.. Fleming (1983) J. Chem. Phys. **79**, 3173–3173.
30. G. R. Fleming (1986) *Chemical Applications of Ultrafast Spectroscopy*, International Series of Monographs on Chemistry, Vol. 13, Oxford University Press, New York.
31. A. J. Ruggiero, D. C. Todd, and G. R. Fleming (1990) *J. Am. Chem. Soc.* **112**, 1003–1014.
32. J. R. Platt (1949) *J. Chem. Phys.* **17**, 484–495.
33. L. J. Andrews and L. S. Forster (1974) *Photochem. Photobiol.* **19**, 353–360.
34. A. Szabo (1984) *J. Chem. Phys.* **81**, 150–167.
35. S. Takeuchi and T. Tahara (1998) *J. Phys. Chem. A* **102**, 7740–7753.
36. T. Ganguly, L. Farmer, D. Gravel, and G. Durocher (1991) *J. Photochem. Photobiol. A Chem.* **60**, 63–82.
37. J. R. Platt (1950) *J. Chem. Phys.* **18**, 1168–1173.
38. To reproduce the simulated $r(t)$ profiles reported by Fleming *et al.* [31], the terms for λ_1 and λ_2 have to be redefined slightly as given by Eqs. (7) and (8).
39. M. Abramowitz and I. A. Stegun (Eds.) (1970) *Handbook of Mathematical Functions*, Dover, New York.
40. It was found that removing this assumption by making k_b^r and k_b^{nr} additional adjustable parameters made very little difference to the conclusions drawn from the analysis, in particular, the value for k_{ba}.
41. J. R. Knutson, J. Beecham, and L. Brand (1983) *Chem. Phys. Lett.* **102**, 501–507.
42. C. A. Langhoff and G. W. Robinson (1974) *Chem. Phys.* **6**, 34–53.
43. G. Bartocci, U. Mazzucato, A. Spalletti, and F. Elisei (1990) *Spectrochim. Acta* **46A**, 413–418.
44. M. Kasha (1950) *Disc. Faraday Soc.* **9**, 14–19.